Fluid Structure Interaction by means of Variational Multiscale Reduced Order Models

Alexis Tello Ramon Codina Joan Baiges

January 24, 2019

Abstract

A stabilized Reduced Order Model (ROM) formulation by means of Variational Multi-Scale (VMS) and an orthogonal projection of the residual has been applied successfully to Fluid-Structure Interaction (FSI) problems in a strongly coupled partitioned solution scheme in non-linear scenarios. Details of the implementation both for the interaction problem and for the reduced model, for both the off-line and on-line phases, are shown. Results are obtained for cases in which both domains are reduced at the same time. Numerical results are presented for a semi-stationary and a fully transient case.

Keywords: Fluid Structure Interaction (FSI), Reduced Order Model (ROM), Variational Multi-Scale Method (VMS), Orthogonal Sub-grid Scale (OSS), Arbitrary Lagrangian Eulerian (ALE), Non-linear Solid Elasto-dynamics

Introduction

Fluid Structure Interaction (FSI) is a topic of constant research and development; and even though fluid and solid formulations might be well understood, FSI remains a complex problem owing to factors as the added mass effect, general instabilities, and the overall conditioning of the problem. Broadly, research in the field can be grouped into two categories based on how the mesh is treated, namely conforming and non conforming methods. Essentially conforming mesh methods consider interface conditions as physical boundary conditions, thus treating the interface as part of the solution. In this approach, the mesh reproduces or conforms to the interface; when the interface is moved it is also necessary to displace the mesh, which carries on all related problems of mesh recalculation and inherent instabilities of the method, be it partitioned or monolithic, see [**Badia2008**, **Farhat2014**, **Farhat2006**, **Bord2013**, **Bazilevs2006**, **Bazilevs2008**, **LeTallec2001**]. On the other hand non-conforming methods treat the interface and boundary as constraints imposed on the governing equations which makes it possible to use meshes that do not reproduce the interface; the main problems being the treatment of the interface conditions and the complexity of the formulation, see for example [**Baiges2017**, **Glowinski2017**] for further reading. For a general review of significant FSI advances and developments see [**Hou2012**]. Overall, for highly non-linear problems, arriving to a solution can a take a large amount of time, an issue that becomes even more apparent when dealing with problems with high number of degrees of freedom. It is well known that ROM can speed up solution time dramatically, which leads to the idea of introducing it into FSI analysis.

Model Order Reduction (MOR) was originally developed for the area of system control theory,

its main purpose being reducing its complexity while maintaining the input-output behavior. The resulting mathematical approximation to the original full order problem is known as a Reduced Order Model ROM. From this, MOR rapidly spread to other fields of research quite successfully. Various ways to achieve model reduction and achieve solution speed up are available, see [**Baiges2013**, **Baiges2013b**, **Schilders2008**, **Sirovich1987**, **Everson1995**]. From this moment on, Proper Orthogonal Decomposition (POD) gained considerable attention in the area of numerical analysis, particularly on fluid dynamics because of its applicability to non linear partial differential equations, It is the foundation of the methods used in this work. In terms of recent FSI-ROM work, we can include [**Colciago2018**] where fluid domain hyper reduction is obtained by means of POD-Greedy algorithms applied to the field of haemodynamics. [**Ballarin2016**] propose a POD approach for a monolithic FSI where the base for said system is obtained in a monolithic way both for Newtonian fluid and linear elastic solid. The idea of their method is the parametrization of variables by means of empirical interpolations providing accurate results for a range of data considered in the interpolation charts. In [**Xiao2016**] the authors introduce the concept of non intrusive model reduction to the FSI field, making the calculation of the reduced basis problem independent. In terms of solid domain reduction, in [**Thari2017**] the authors apply modal analysis by means of model recalibration to the movement of a membrane.

Our approach is different, we propose the reduced system to be variational by nature and use the need of stabilization as a way to project the solution of both fluid and solid onto the reduced space. This is not the first time this is done however, see for example [**Baiges2014**], where the idea of sub-scales is first explored, [**Giere2015**] where for the first time stabilization trough the residual of the reduced space is considered, and finally [**Reyes2018**] where the residual of the reduced problem is projected into the reduced space where the solution is though to live in; we apply this formulation in this work.

The paper is organized as follows: in the first sections we describe each particular formulation (fluid and solid) in a short manner, followed by the introduction of FSI. Afterwards an overview of ROM will be given, detailing our implementation to finally conclude with numerical results.

1 Incompressible Navier-Stokes equations

In the next section we give an overview of the incompressible Navier-Stokes equations and the way we stabilize them.

1.1 Governing equations

For a certain domain Ω_{fl} with boundary $\Gamma_{\mathrm{fl}} = \Gamma_{\mathrm{D,fl}} \cup \Gamma_{\mathrm{N,fl}}$, where $\Gamma_{\mathrm{D,fl}}$ and $\Gamma_{\mathrm{N,fl}}$ are boundaries where Dirichlet and Neumann conditions are prescribed, respectively, let $]0, t_{\mathrm{f}}[$ the time interval of analysis, the incompressible Navier-Stokes equations can be written as; find a pair $[\boldsymbol{u}, p] : \Omega_{\mathrm{fl}} \times]0, t_{\mathrm{f}}[\longrightarrow \mathbb{R}^d \times \mathbb{R}$, where d is the space dimension, such that the solution to the following equations can be

obtained:

$$\begin{aligned}
\rho_{\mathrm{fl}}\partial_t \boldsymbol{u} - 2\mu\nabla\cdot\nabla^s\boldsymbol{u} + \rho_{\mathrm{fl}}\boldsymbol{u}\cdot\nabla\boldsymbol{u} + \nabla p &= \boldsymbol{f} && \text{in } \Omega_{\mathrm{fl}}, && t\in\,]0,t_{\mathrm{f}}[,\\
\nabla\cdot\boldsymbol{u} &= 0 && \text{in } \Omega_{\mathrm{fl}}, && t\in\,]0,t_{\mathrm{f}}[,\\
\boldsymbol{u} &= \boldsymbol{u}_{\mathrm{D}} && \text{on } \Gamma_{\mathrm{D,fl}}, && t\in\,]0,t_{\mathrm{f}}[,\\
\boldsymbol{n}_{\mathrm{fl}}\cdot\boldsymbol{\sigma}_{\mathrm{fl}} &= \boldsymbol{t}_{\mathrm{fl}} && \text{on } \Gamma_{\mathrm{N,fl}}, && t\in\,]0,t_{\mathrm{f}}[,\\
\boldsymbol{u} &= \boldsymbol{u}^0 && \text{in } \Omega_{\mathrm{fl}}, && t=0,
\end{aligned}$$

where μ is the fluid's dynamic viscosity, $\boldsymbol{f}$ is the force vector, $\boldsymbol{\sigma}_{\mathrm{fl}}$ is the fluid's stress tensor, $\boldsymbol{u}^0$ is a prescribed initial velocity, $\boldsymbol{u}_{\mathrm{D}}$ is a prescribed velocity on the boundary $\Gamma_{\mathrm{D,fl}}$, $\boldsymbol{t}_{\mathrm{fl}}$ is a prescribed traction on the boundary $\Gamma_{\mathrm{N,fl}}$, and $\boldsymbol{n}_{\mathrm{fl}}$ is the normal to the fluid domain.
Now we proceed to define the finite element space where the weak form of these equations makes sense.

1.2 Weak form

Let us start by introducing some standard notation that will be used all throughout this work. The space of functions whose p power ($p \geq 1$) is integrable in a domain Ω is denoted by $L^p(\Omega)$, and the space of functions whose distributional derivatives of order up to $m \geq 0$ belong to $L^2(\Omega)$ by $H^m(\Omega)$, we denote the duality pairing as $\langle\cdot,\cdot\rangle$. The L^2 inner product in Ω (for scalars, vectors or tensor) is denoted by $(\cdot,\cdot)$ and the norm in a Banach space X by $||\cdot||_X$
Using this notation the velocity and pressure finite element spaces for the continuous problem are $\mathscr{V}_0 = \{\boldsymbol{v} \in H^1(\Omega) \mid \boldsymbol{v}|_{\Gamma_D} = \boldsymbol{0}\}$, $\mathscr{Q} = L^2(\Omega)$ respectively. We are also interested in the spaces $\mathscr{W}_0 = \mathscr{V}_0 \times \mathscr{Q}$, $\mathscr{V}_D = \{\boldsymbol{v} \in H^1(\Omega) \mid \boldsymbol{v}|_{\Gamma_D} = \boldsymbol{u}_D\}$,$\mathscr{W}_D = \mathscr{V}_D \times \mathscr{Q}$.
The weak form of the Navier-Stokes equations consists in finding $[\boldsymbol{u}, p] \in L^2(0,t_{\mathrm{f}};\mathscr{V}_D)\times L^1(0,t_{\mathrm{f}};\mathscr{Q})$ such that

$$\begin{aligned}
(\rho_{\mathrm{fl}}\partial_t\boldsymbol{u},\boldsymbol{v}) - 2\mu(\nabla^s\boldsymbol{u},\nabla^s\boldsymbol{v})&\\
+\rho_{\mathrm{fl}}\langle\boldsymbol{u}\cdot\nabla\boldsymbol{u},\boldsymbol{v}\rangle - (p,\nabla\cdot\boldsymbol{v}) =& \langle\boldsymbol{f},\boldsymbol{v}\rangle + \langle\boldsymbol{t},\boldsymbol{v}\rangle_{\Gamma_{N,fl}}, && t\in\,]0,t_{\mathrm{f}}[,\\
(q,\nabla\cdot\boldsymbol{u}) =& 0, && t\in\,]0,t_{\mathrm{f}}[,\\
(\boldsymbol{u},\boldsymbol{v}) =& (\boldsymbol{u}^0,\boldsymbol{v}), && t=0,
\end{aligned} \tag{1}$$

for all $[\boldsymbol{v}, q] \in \mathscr{V}_0 \times \mathscr{Q}$ and satisfying initial conditions in a weak sense. It is possible to define a form B as:

$$B(\boldsymbol{U},\boldsymbol{V}) = 2\mu(\nabla^s\boldsymbol{u},\nabla^s\boldsymbol{v}) + \rho_{\mathrm{fl}}\langle\boldsymbol{u}\cdot\nabla\boldsymbol{u},\boldsymbol{v}\rangle - (p,\nabla\cdot\boldsymbol{v}) + (q,\nabla\cdot\boldsymbol{u}), \tag{2}$$

and a linear form as,

$$L(\boldsymbol{V}) = \langle\boldsymbol{f},\boldsymbol{v}\rangle + \langle\boldsymbol{t},\boldsymbol{v}\rangle_{\Gamma_{N,fl}}, \tag{3}$$

which enables us to write equation (1) in the following simplified form,

$$(\rho_{\mathrm{fl}}\partial_t\boldsymbol{u},\boldsymbol{v}) + B(\boldsymbol{U},\boldsymbol{V}) = L(\boldsymbol{V}), \forall\, \boldsymbol{V} \in \mathscr{W}_0, \tag{4}$$

for $\boldsymbol{U} \equiv [\boldsymbol{u}, p] :]0,t_{\mathrm{f}}[\longrightarrow \mathscr{W}_D$ and $\boldsymbol{V} \equiv [\boldsymbol{v}, q] \in \mathscr{W}_0$, where initial conditions should hold.

1.3 Spatial discretization

For the spatial discretization the standard Galerkin finite elements approximation can be defined as follows. Let $\mathscr{P}_h$ denote a finite element partition of the domain Ω. The diameter of an element domain $K \in \mathscr{P}$ is denoted by h_k and the diameter of the finite element partition by

$h = \max\{h_K | K \in \mathscr{P}\}$. We can now construct conforming finite element spaces $\mathscr{V}_h \subset \mathscr{V}_D$, $\mathscr{Q}_h \subset \mathscr{Q}$ and $\mathscr{W}_{h,D} = \mathscr{V}_h \times \mathscr{Q}_h$ as well as the corresponding sub-spaces $\mathscr{V}_{h,0}$, $\mathscr{Q}_{h,0}$ and $\mathscr{W}_{h,0} = \mathscr{V}_{h,0} \times \mathscr{Q}_{h,0}$. Then the problem can be written as: find $\boldsymbol{U}_h :]0, t_\mathrm{f}[\longrightarrow \mathscr{W}_{h,D}$ as the solution to the problem,

$$\begin{aligned} (\rho_\mathrm{fl} \partial_t \boldsymbol{u}_h, \boldsymbol{v}_h) + B(\boldsymbol{U}_h, \boldsymbol{V}_h) &= L(\boldsymbol{V}_h), & \forall\, \boldsymbol{V}_h \in \mathscr{W}_{h,0} \\ (\boldsymbol{u}_h, \boldsymbol{v}_h) &= (\boldsymbol{u}^0, \boldsymbol{v}_h) & \forall\, \boldsymbol{v}_h \in \mathscr{V}_{h,0}, \end{aligned} \tag{5}$$

1.4 Time discretization

Let us consider a uniform partition of the time interval $]0, t_\mathrm{f}[$ of size Δt, and let us denote with superscript n the time interval level. For the temporal discretization usual finite difference schemes are adopted. In particular the Backward Euler (BE) or the second order Backward Differences scheme (BDF2) which has the following form:

$$\frac{\partial \boldsymbol{u}_h^{n+1}}{\partial t} = \frac{3\boldsymbol{u}_h^{n+1} - 4\boldsymbol{u}_h^n + \boldsymbol{u}_h^{n-1}}{\Delta t} + \mathscr{O}(\Delta t^2), \tag{6}$$

where n is the current time step counter.

1.5 Stabilization

To circumvent the restrictions imposed by the inf-sup condition and convection dominated flows, a variational multi-scale stabilization is applied, originally proposed on [**Hughes1998**] and later further developed in [**Codina2000**, **Codina2002**]. When applied to the Navier-Stokes problem problem equation (5) can be replaced by,

$$\begin{aligned} &(\rho_\mathrm{fl} \partial_t \boldsymbol{u}_h^{n+1}, \boldsymbol{v}_h) + B(\boldsymbol{U}_h^{n+1}, \boldsymbol{V}_h) + \left(\Pi^\perp \left(\boldsymbol{r}\left(\boldsymbol{U}_h^{n+1}\right)\right), \boldsymbol{u}_h^{n+1} \cdot \nabla \boldsymbol{v}_h + \nu \Delta \boldsymbol{v}_h + \nabla q_h \right)_{\tau_{1,t}} \\ &\quad + \left(\Pi^\perp \left(\nabla \cdot \boldsymbol{u}_h^{n+1} \right), \nabla \cdot \boldsymbol{v}_h \right)_{\tau_2} = L(\boldsymbol{V}_h) + \frac{1}{\Delta t} \left(\widetilde{\boldsymbol{u}}^n, \boldsymbol{u}_h^n \cdot \nabla \boldsymbol{v}_h + \nu \Delta \boldsymbol{v}_h + \nabla q_h \right), \end{aligned} \tag{7}$$

where $\boldsymbol{r}\left(\boldsymbol{U}_h^{n+1}\right) = \partial_t \boldsymbol{u}_h^{n+1} - \nu \Delta \boldsymbol{u}_h^{n+1} + \boldsymbol{u}_h^{n+1} \cdot \nabla \boldsymbol{u}_h^{n+1} + \nabla p_h^{n+1} - \boldsymbol{f}_h^{n+1}$, is the residual of the momentum equation, $\Pi^\perp$ is the projection of $\boldsymbol{r}\left(\boldsymbol{U}_h^{n+1}\right)$ to the orthogonal space of subscales $\widetilde{\boldsymbol{u}}$, and $\tau_{1,t}$ and τ_2 the stabilization parameters:

$$\tau_{1,t} = \left(\frac{1}{\Delta t} + \frac{1}{\tau_1} \right)^{-1}, \tag{8a}$$

$$\tau_1 = \left[\left(c_1 \frac{\nu}{h^2} \right)^2 + \left(c_2 \frac{|\boldsymbol{u}_h|_K}{h} \right)^2 \right]^{-1}, \tag{8b}$$

$$\tau_2 = c_3 \frac{h^2}{\tau_1}, \tag{8c}$$

where $|\boldsymbol{u}_h|_K$ is the mean velocity modulus in element K, h is the element size and c_1, c_2 and c_3 are stabilization constants and $(\boldsymbol{X}, \boldsymbol{Y})_\tau = (\tau \boldsymbol{X}, \boldsymbol{Y}) = (\boldsymbol{X}, \tau \boldsymbol{Y})$ is understood as the weighted inner product by τ. Note that the sub-scales, for our particular case, evolve through time $\widetilde{\boldsymbol{u}}(t)$, their solution can be found in [**Codina2002**]. For linear elements we take $c_1 = 4.0$, $c_2 = 2.0$ and $c_3 = 1.0$. For quadratic elements we use the same values but taking h half the element size (roughly the distance between nodes of the element), as justified in [**Codina2001**].

2 Non-Linear solid elasto-dynamics

In this section a short review of non-linear solid elasto-dynamics is given as well as the spatial and temporal discretization schemes used.

2.1 Governing equations

For a certain domain Ω_s with boundary $\Gamma_\mathrm{s} = \Gamma_{\mathrm{D,s}} \cup \Gamma_{\mathrm{N,s}}$, where $\Gamma_{\mathrm{D,s}}$ and $\Gamma_{\mathrm{N,s}}$ are boundaries where Dirichlet and Neumann conditions are prescribed, respectively, let $]0, t_\mathrm{f}[$ the time interval of analysis, the elasto-dynamic problem written in updated Lagrangian form, see for example [**Belytschko2014**], consists in finding a displacement $\boldsymbol{d} : \Omega_\mathrm{s} \times]0, t_\mathrm{f}[\longrightarrow \mathbb{R}^d$ such that:

$$
\begin{aligned}
\rho_\mathrm{s} \partial_{tt} \boldsymbol{d} - \nabla \cdot \boldsymbol{\sigma}_s = \rho_\mathrm{s} \boldsymbol{f} \quad & \text{in } \Omega_\mathrm{s}, \quad && t \in]0, t_\mathrm{f}[, \\
\boldsymbol{d} = \boldsymbol{d}_\mathrm{D} \quad & \text{on } \Gamma_{\mathrm{D,s}}, \quad && t \in]0, t_\mathrm{f}[, \\
\boldsymbol{n}_\mathrm{s} \cdot \boldsymbol{\sigma}_\mathrm{s} = \boldsymbol{t}_\mathrm{s} \quad & \text{on } \Gamma_{\mathrm{N,s}}, \quad && t \in]0, t_\mathrm{f}[, \\
\partial_t \boldsymbol{d} = \dot{\boldsymbol{d}}^0 \quad & \text{in } \Omega_\mathrm{s}, \quad && t = 0, \\
\boldsymbol{d} = \boldsymbol{d}^0 \quad & \text{in } \Omega_\mathrm{s}, \quad && t = 0,
\end{aligned}
\tag{9}
$$

where ρ_s is the solid's density, $\boldsymbol{\sigma}_\mathrm{s}$ is the solid's Cauchy stress tensor, $\boldsymbol{f}_\mathrm{s}$ is the force vector, $\boldsymbol{d}^0$ is a prescribed initial displacement and $\dot{\boldsymbol{d}}^0$ is a prescribed initial velocity, $\boldsymbol{d}_D$ is a prescribed displacement on the boundary $\Gamma_{\mathrm{D,s}}$, $\boldsymbol{t}_\mathrm{s}$ is a prescribed traction on the boundary $\Gamma_{\mathrm{N,s}}$, and $\boldsymbol{n}_\mathrm{s}$ is the normal to the solid domain.

In the non-linear setting the constitutive equation for the stress tensor can be modeled in a variety of ways and depends on the material to be simulated. In the present case we are interested in the Neo-Hookean and Saint Venant-Kirchoff material models, which can be defined as follows,

$$
\begin{aligned}
\text{NeoHookean} \;\; \boldsymbol{\sigma} &= \frac{1}{J} \left[\lambda \ln(J) \mathbb{I} + \mu (\boldsymbol{b} - \mathbb{I}) \right] \\
\text{Saint Venant-Kirchoff} \;\; \boldsymbol{\sigma} &= \frac{1}{J} \boldsymbol{F} \left[\lambda \mathrm{tr}(\boldsymbol{E}) \mathbb{I} + 2\mu \boldsymbol{E} \right] \boldsymbol{F}^T,
\end{aligned}
$$

where $\boldsymbol{F} = \frac{\partial \boldsymbol{x}}{\partial \boldsymbol{X}}$ is the material deformation gradient, $J = \det(\boldsymbol{F})$, λ and μ are Lamé's parameters, $\boldsymbol{b} = \boldsymbol{F}\boldsymbol{F}^T$ is the left Cauchy tensor, $\mathbb{I}$ is the identity tensor and $\boldsymbol{E}$ is Green strain tensor.

2.2 Weak form

Making use of the spaces and operators defined in section 1.2 we can define the non linear elasto-dynamic problem in the following way,

Let $\mathscr{E}_0 := \{\boldsymbol{e} \in H^1(\Omega) \mid \boldsymbol{e}|_{\Gamma_D} = \boldsymbol{0}\}$. We are also interested in the spaces $\mathscr{E}_D = \{\boldsymbol{e} \in H^1(\Omega) \mid \boldsymbol{e}|_{\Gamma_D} = \boldsymbol{d}_D\}$. Hence, the weak form of the solid elasto-dynamic problem consists in finding $\boldsymbol{d} \in L^2(0, t_\mathrm{f}; \mathscr{E}_D)$ such that:

$$
\begin{aligned}
(\rho_\mathrm{s} \partial_{tt} \boldsymbol{d}, \boldsymbol{e}) - (\boldsymbol{\sigma}, \nabla^s \boldsymbol{e}) = \langle \rho_\mathrm{s} \boldsymbol{f}, \boldsymbol{e} \rangle + \langle \boldsymbol{t}_\mathrm{s}, \boldsymbol{e} \rangle_\Gamma \quad & t \in]0, t_\mathrm{f}[, \\
(\partial_t \boldsymbol{d}, \boldsymbol{e}) = (\dot{\boldsymbol{d}}^0, \boldsymbol{e}), \quad & t \in]0, t_\mathrm{f}[, \\
(\boldsymbol{d}, \boldsymbol{e}) = (\boldsymbol{d}^0, \boldsymbol{e}), \quad & t \in]0, t_\mathrm{f}[,
\end{aligned}
\tag{10}
$$

for all $\boldsymbol{e} \in \mathscr{E}_0$.

2.3 Spatial discretization

We can discretize the solid domain as done for the fluid, and use also an analogous notation. In this way we can now construct conforming finite element spaces $\mathscr{E}_h \subset \mathscr{E}_\mathrm{D}$ as well as the corresponding subspaces $\mathscr{E}_{h,0}$ and $\mathscr{E}_{h,D}$. Then the problem can be written as, find $\boldsymbol{d} \in L^2(0, t_\mathrm{f}; \mathscr{E}_{h,D})$ such that:

$$\begin{aligned}(\rho_\mathrm{s}\partial_{tt}\boldsymbol{d}_h, \boldsymbol{e}_h) - (\boldsymbol{\sigma}_h, \nabla^s \boldsymbol{e}_h) &= \langle \rho_\mathrm{s}\boldsymbol{f}_h, \boldsymbol{e}_h\rangle + \langle \boldsymbol{t}_{h,s}, \boldsymbol{e}_h\rangle_{\Gamma_{\mathrm{N},\mathrm{s}}}, \\ (\partial_t \boldsymbol{d}_h(0), \boldsymbol{e}_h) &= (\dot{\boldsymbol{d}}^0, \boldsymbol{e}_h), \\ (\boldsymbol{d}_h(0), \boldsymbol{e}_h) &= (\boldsymbol{d}^0, \boldsymbol{e}_h),\end{aligned} \tag{11}$$

for all $\boldsymbol{e}_h :]0, t_\mathrm{f}[\longrightarrow \mathscr{E}_{h,0}$ and satisfying initial conditions in a weak sense. This problem can be linearized using a Newton-Raphson scheme; for further detail see for example [**Belytschko2014**].

2.4 Time discretization

For the temporal discretization the following second order Backward Differences scheme (BDF2) has been used,

$$\boldsymbol{a}^{n+1} = \frac{1}{(\Delta t)^2}\left(2\boldsymbol{d}^{n+1} - 5\boldsymbol{d}^n + 4\boldsymbol{d}^{n-1} - \boldsymbol{d}^{n-2}\right),$$

where $\boldsymbol{d}^{n+1}$ and $\boldsymbol{a}^{n+1}$ are approximations to the position and acceleration vectors at time step $n+1$.

3 Fluid Structure Interaction

Once all ingredients have been identified it is possible to detail the process of dealing with FSI problems. In this section we first express the FSI equations in weak form, and we detail the FSI algorithm as well as boundary relaxation scheme used.

3.1 Governing equations and weak form

The approach followed in this work can be taken as the traditional in a broad sense, where an updated Lagrangian formulation is used to deal with the solid mechanics problem while the fluid problem is solved by means of an Arbitrary-Lagrangian-Eulerian formulation. [**Donea1999**] explains in a very detailed manner the ALE formulation, as well as its advantages and disadvantages. The mesh movement algorithm has been taken from [**Chiandussi2000**], which has proven simple, robust and reliable.

Borrowing from the notation developed in previous sections we can expand it to account for a moving domain and to take into account the interaction between sub-domains. For the FSI problem the space for the continuous problem can be defined as $\mathscr{F}_{D,t} = \mathscr{W}_{D,t} \times \mathscr{E}_{D,t}$, and the fluid structure

interaction problem can be stated as: find $[\boldsymbol{u}, p, \boldsymbol{d}] \in L^2(0, t_\mathrm{f}; \mathscr{V}_{D,t}) \times L^1(0, t_\mathrm{f}; \mathscr{Q}_{D,t}) \times L^2(0, t_\mathrm{f}; \mathscr{E}_{D,t})$ such that

$$
\begin{aligned}
\rho_\mathrm{fl}(\partial_t \boldsymbol{u}, \boldsymbol{v}) - 2\mu(\nabla^s \boldsymbol{u}, \nabla^s \boldsymbol{v}) & \\
+\rho_\mathrm{fl}\langle \boldsymbol{c} \cdot \nabla \boldsymbol{u}, \boldsymbol{v}\rangle - (p, \nabla \boldsymbol{v}) = \langle \boldsymbol{f}, \boldsymbol{v}\rangle + \langle \boldsymbol{t}_\mathrm{fl}, \boldsymbol{v}\rangle_{\Gamma_{\mathrm{N,fl}}} & \quad \text{in } \Omega(t)_\mathrm{fl},\ t\ \in]0, t_\mathrm{f}[\\
(q, \nabla \cdot \boldsymbol{u}) = 0 & \quad \text{in } \Omega(t)_\mathrm{fl},\ t\ \in]0, t_\mathrm{f}[\\
(\rho_\mathrm{s} \partial_{tt} \boldsymbol{d}, \boldsymbol{e}) - (\boldsymbol{\sigma}, \nabla^s \boldsymbol{e}) = \langle \rho_\mathrm{s} \boldsymbol{f}, \boldsymbol{e}\rangle + \langle \boldsymbol{t}_\mathrm{s}, \boldsymbol{e}\rangle_{\Gamma_{\mathrm{N,s}}} & \quad \text{in } \Omega(t)_\mathrm{s},\ t\ \in]0, t_\mathrm{f}[\\
\boldsymbol{u} = \partial_t \boldsymbol{d} & \quad \text{on } \Gamma(t)_\mathrm{I},\ t\ \in]0, t_\mathrm{f}[\\
\boldsymbol{n}_\mathrm{s} \cdot \boldsymbol{\sigma}_\mathrm{s} = \boldsymbol{n}_\mathrm{fl} \cdot \boldsymbol{\sigma}_\mathrm{fl} & \quad \text{on } \Gamma(t)_\mathrm{I},\ t\ \in]0, t_\mathrm{f}[,
\end{aligned}
\tag{12}
$$

for all $[\boldsymbol{v}, q, \boldsymbol{e}] \in \mathscr{F}_{0,t}$, with $\mathscr{F}_{0,t} = \mathscr{W}_{0,t} \times \mathscr{E}_{0,t}$, and satisfying initial conditions in a weak sense. Here, $\boldsymbol{c}$ is known as the convection velocity from the mesh point of view. Also note that in this form, the domain to which the fluid and solid pertains, $\Omega(t)_\mathrm{fl}$ and $\Omega(t)_\mathrm{s}$, respectively, is now time dependent as it changes according to the deformation process. $\Gamma(t)_\mathrm{I}$ is the interface boundary for both domains, as shown in Figure 1.

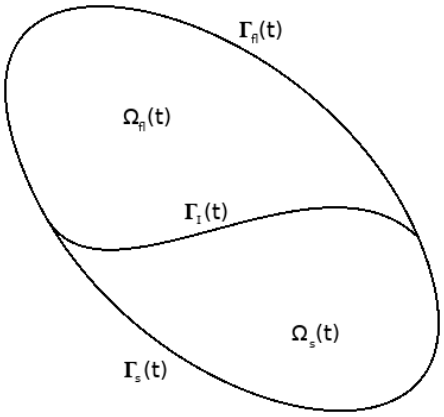

Figure 1: Domain composed of two different sub-domains, $\Omega_\mathrm{fl}(t)$ and $\Omega_\mathrm{s}(t)$, their interface $\Gamma_\mathrm{I}(t)$ and respective boundaries $\Gamma_\mathrm{fl}(t)$ and $\Gamma_\mathrm{s}(t)$

3.1.1 Coupling scheme

The are various ways to treat the numerical system from the interaction problem regardless of the particular formulation used to solve each domain; In a monolithic coupling the whole problem is assembled and solved from one matrix. Coupling is treated implicitly through the left hand side of the system, see for example [**Fan2018**, **Sauer2018**], this approach benefits from increased stability on the solution but requires more specialized solvers that can deal with less than optimally scaled numerical systems. On the other hand, partitioned approaches assemble each domain independently and coupling is achieved through the right hand side terms of each system; for strongly coupled systems sub-iterations, and very often relaxation, are necessary to guarantee quantity convergence on the interaction boundaries. In some cases, a high number of coupling iterations are necessary to achieve convergence, see [**Akbay2018**, **Langer2015**]. Finally a less popular approach is by means of a staggered coupling (or loosely coupled interaction), this is essentially a partitioned approach where the boundary conditions are treated explicitly and no sub-iterations are done, this approach can suffer from instabilities, like added mass effect, see [**Fo2007**].

We apply a partitioned, strongly coupled, scheme to achieve domain coupling; this means that for every time-step each domain is iterated independently until convergence is achieved for velocity, pressure and displacement for the interaction boundary. This creates the necessity of an additional convergence block that guarantees coupling convergence. In total we are left with four coupling blocks, this being, the internal solver convergence, the non-linearity convergence (in the case of the fluid for the convective term as a Picard iterative scheme is applied), the coupling convergence for the interaction boundary and finally the temporal convergence for a given time step. To clarify this is shown in section 3.1.2. In our implementation iteration by sub-domain can be done for non matching meshes by means of the usual Lagrange interpolation functions as shown in [**Houzeaux2001**].

It is essential to guarantee correct interface coupling as mesh displacements and velocities should be up to a certain tolerance equivalent. This can be achieved by means of simple sub-iteration until quantities converge but due to the non-linear nature of the problem relaxation is very often required if not mandatory. Dynamic sub-relaxation is an efficient way to minimize the amount of sub-iterations necessary to achieve boundary convergence as the relaxation coefficient is calculated by means of a minimization problem and not simply as user input. We implement an Aitken relaxation scheme, in particular Aitken Δ^2, detailed in [**Kuttler2008**]. The relaxation parameter ω_i is obtained as follows,

For a given time step $n+1$ and a coupling iteration $k+1$:

- Calculate interface displacement residual, $\boldsymbol{r}_{\Gamma_{\mathrm{I}},k+1} = \boldsymbol{r}_{\Gamma_{\mathrm{I}},k} - \widetilde{\boldsymbol{r}}_{\Gamma_{\mathrm{I}},k+1}$,
- Compute Aitken coefficient: $\omega_{k+1} = -\omega_k \frac{(\boldsymbol{r}_{\Gamma_{\mathrm{I}},k+1})^T(\boldsymbol{r}_{\Gamma_{\mathrm{I}},k+2} - \boldsymbol{r}_{\Gamma_{\mathrm{I}},k+1})}{|\boldsymbol{r}_{\Gamma_{\mathrm{I}},k+2} - \boldsymbol{r}_{\Gamma_{\mathrm{I}},k+1}|^2}$,

where k is the current coupling iteration, $\widetilde{\boldsymbol{r}}_{\Gamma_{\mathrm{I}},k+1} = (\boldsymbol{d}_{\mathrm{s}} - \boldsymbol{d}_{\mathrm{mesh}})_{\Gamma_{\mathrm{I}},k+1}$ is the current residual between solid and mesh displacement for the interaction boundary.

3.1.2 General FSI algorithm

For a time interval between 0 and t_{f}, let n be the current time step, n_{last} the last time step, i the current internal iteration of a particular sub-domain (fluid or solid), k the current coupling iteration for both domains, $\mathrm{Tol}_{\mathrm{time}}$ the temporal tolerance, $\mathrm{Tol}_{\mathrm{cou}}$ the coupling tolerance between sub-domains, $\mathrm{Tol}_{\mathrm{s}}$ the internal tolerance for convergence for the solid sub-domain, $\mathrm{Tol}_{\mathrm{fl}}$ the internal tolerance for convergence for the fluid sub-domain. The FSI algorithm reads:

Read case parameters and initialize values for fluid and solid domains
for $n = 1; n \leq n_{\text{last}}; n+1$ **do**
  for $k = 1; k \leq k_{\max}; k+1$ **do**
    Calculate relaxation parameter ω_{k+1} for Γ_{I} from $\boldsymbol{r}_{\Gamma_{\text{I}},k+1}$
    Calculate mesh interface movement $\boldsymbol{d}_{\Gamma_{\text{I}}}^{k+1} = \boldsymbol{d}_{\Gamma_{\text{I}}}^{k} + \omega_{k+1}\boldsymbol{r}_{\Gamma_{\text{I}},k+1}$
    Calculate mesh movement $\boldsymbol{d}_{\text{mesh}}^{k+1}$ and velocity $\boldsymbol{u}_{\text{mesh}}^{k+1}$ from $\boldsymbol{d}_{\Gamma_{\text{I}}}^{k+1}$
    for $i = 1; i \leq i_{\max}; i+1$ **do**
      Solve Fluid domain for $[\boldsymbol{u}, p]^{i+1}$ from $\boldsymbol{u}_{\text{mesh}}^{k+1}$
      Calculate tractions $\boldsymbol{t}_{\text{fl}}$ on Γ_{I}
      Calculate error $\epsilon_{\boldsymbol{u}}^{i+1} = \frac{|\boldsymbol{u}^{i+1} - \boldsymbol{u}^{i}|}{|\boldsymbol{u}^{i+1}|}$; $\epsilon_{p}^{i+1} = \frac{|p^{i+1} - p^{i}|}{|p^{i+1}|}$;
      if $\epsilon_{\boldsymbol{u}}^{i+1}$ and $\epsilon_{\boldsymbol{p}}^{i+1} \leq \text{Tol}_{\text{fl}}$ **then**
        Non linearity converged; Break non-linearity loop
      end if
    end for
    for $i = 1; i \leq i_{\max}; i+1$ **do**
      Solve Solid domain for $\boldsymbol{d}^{i+1}$ from $\boldsymbol{t}_{\text{fl}}$
      Calculate error $\epsilon_{\boldsymbol{d}}^{i+1} = \frac{|\boldsymbol{d}^{i+1} - \boldsymbol{d}^{i}|}{|\boldsymbol{d}^{i+1}|}$
      if $\epsilon_{\boldsymbol{d}}^{i+1} \geq \text{Tol}_{\text{s}}$ **then**
        Non linearity converged; Break non-linearity loop
      end if
    end for
    Calculate coupling error $\epsilon_{\boldsymbol{u}}^{k+1} = \frac{|\boldsymbol{u}^{k+1} - \boldsymbol{u}^{k}|}{|\boldsymbol{u}^{k+1}|}$; $\epsilon_{p}^{k+1} = \frac{|p^{k+1} - p^{k}|}{|p^{k+1}|}$; $\epsilon_{\boldsymbol{d}}^{k+1} = \frac{|\boldsymbol{d}^{k+1} - \boldsymbol{d}^{k}|}{|\boldsymbol{d}^{k+1}|}$
    if $\epsilon_{\boldsymbol{u}}^{k+1}$ and ϵ_{p}^{k+1} and $\epsilon_{\boldsymbol{d}}^{k+1}$ on $\Gamma_{\text{I}} \leq \text{Tol}_{\text{coup}}$ **then**
      Coupling converged; Break Coupling loop
    end if
  end for
  Calculate temporal error $\epsilon_{\boldsymbol{u}}^{n+1} = \frac{|\boldsymbol{u}^{n+1} - \boldsymbol{u}^{n}|}{|\boldsymbol{u}^{n+1}|}$; $\epsilon_{p}^{n+1} = \frac{|p^{n+1} - p^{n}|}{|p^{n+1}|}$; $\epsilon_{\boldsymbol{d}}^{n+1} = \frac{|\boldsymbol{d}^{n+1} - \boldsymbol{d}^{n}|}{|\boldsymbol{d}^{n+1}|}$
  if $\epsilon_{\boldsymbol{u}}^{n+1}$ and ϵ_{p}^{n+1} and $\epsilon_{\boldsymbol{d}}^{n+1} \leq \text{Tol}_{\text{time}}$ **then**
    Stationary state achieved; Break temporal loop
  end if
end for
Finalize case
Output if necessary

A case is understood as a problem set, governing equations, boundary conditions, particular solver and any other necessary numerical parameters. This approach allows us to solve in a decoupled manner each problem.

4 Reduced order modeling

As discussed in section 3.1.1, strongly coupled partitioned FSI algorithms may require a high number of sub-iterations and sub-relaxation, making the problem potentially expensive numerically and consequently taking a long time to achieve solution. In this sense development of model order reduction schemes that increase performance while maintaining output accuracy is of interest. Herein lies our motivation to introduce ROM into FSI; In this section we give a short review of the

methodology we apply and the algorithmic aspects that concern it.

4.1 Some ROM theory

Let us define a high dimensional space $\mathscr{Y}_h$ of dimension M, with $\boldsymbol{\varphi}$ its orthonormal basis. Then, the i-th component of any element $\boldsymbol{y}_h \in \mathscr{Y}_h$ can be written as the linear combination $y_{h,i} = \sum_{k=1}^{M} (y_{h,i}, \varphi_i^k)\varphi_i^k$, with $(\cdot,\cdot)$ a L^2-inner product. Since for most cases the exact basis $\boldsymbol{\varphi}$ is unknown, we can define a low-dimensional space $\mathscr{Y}_{\text{rom}} \subset \mathscr{Y}_h$ of dimension m, which approximates $\mathscr{Y}_h$ as $m \to M$, with a basis $\boldsymbol{\phi}$. Using this test basis, we can approximate the i-th component of any element $\boldsymbol{y}_h$ as $y_{h,i} \approx y_{\text{rom},i} = \sum_{k=1}^{m} \phi_i^k a_i^k$, where a_i^k is the $i-th$ coefficient obtained from the solution of the reduced problem; the accuracy of the approximation depends on how accurate is the basis $\boldsymbol{\phi}$ compared to the exact basis $\boldsymbol{\varphi}$.

4.1.1 Construction of the basis

The objective of the Proper Orthogonal Decomposition (POD) method is finding a basis for a collection of high-fidelity 'snapshots' (defined as the solution of the problem taken at a specific time step) to use as the basis of the desired reduced sub-space. Taking a set of data as a N-collection of 'snapshots' $\{\boldsymbol{s}_j\}_{j=1}^N = \{\boldsymbol{y}_{h,j} - \bar{\boldsymbol{y}}_h\}$, we can reproduce any element of said collection as:

$$\boldsymbol{y}_{h,j} \approx \bar{\boldsymbol{y}}_h + \sum_{k=1}^{m} (\boldsymbol{s}_j, \boldsymbol{\phi}^k)\boldsymbol{\phi}^k, \tag{13}$$

where, in the case of POD, $\{\boldsymbol{\phi}^k\}_{k=1}^m$ is an orthonormal basis of $\mathscr{Y}_h$, and $\bar{\boldsymbol{y}}_h$ is the mean value of the snapshots. The POD consists in finding the orthonormal basis $\{\boldsymbol{\phi}^k\}_{k=1}^m$, such that, for every $k \in \{1,\dots,m\}$ the mean square error between the elements $\boldsymbol{y}_{h,j}$, $1 \le j \le N$, and the corresponding j-th partial sum of equation (13) is minimized on average:

$$\begin{aligned} \min_{\{\boldsymbol{\phi}\}_{k=1}^m} \quad & \frac{1}{N}\sum_{j=1}^{N} \left\| \boldsymbol{s}_j - \sum_{k=1}^{m} (\boldsymbol{s}_j, \boldsymbol{\phi}^k)\boldsymbol{\phi}^k \right\|^2, \\ \text{subject to } & (\boldsymbol{\phi}^i, \boldsymbol{\phi}^j) = \delta_{ij}, \quad 1 \le i,j \le m. \end{aligned} \tag{14}$$

By means of a Singular Value Decomposition, or SVD, we can solve for the basis $\{\boldsymbol{\phi}^k\}_{k=1}^m$ from the matrix of snapshots. This basis depends on parameters as time-step, how often a snapshot was acquired and the reproducibility of the function being analyzed. A reduced basis can be defined by truncating the left singular-vectors at the m column as: $\{\boldsymbol{\phi}^k\}_{k=1}^{m \ll M}$. As a criterion for the truncation, we use the retained energy η defined in [**Sirovich1987**] as:

$$\eta = \frac{\sum_{k=1}^{m} \lambda^k}{\sum_{k=1}^{M} \lambda^k}, \tag{15}$$

where λ^k is the SVD non-zero singular values. We term the stage of the problem in which the base is calculated as the off-line phase.

The SVD produces as well a diagonal matrix which contains, from greatest to least, the eigenvalues of the associated basis functions. The ordering of the eigenvalues is a measure of the relative importance of each of the basis functions in the whole system. And in general, in a reducible problem (a problem that should be easily reproduced by means of ROM) they decrease quickly in magnitude. If m is sufficiently small, the time to compute the reduced system is minimal.

Remark. *In the rest of this work a base which contains a greater number of basis vectors than another one will be referred as a 'richer' base.*

Note that the construction of the basis can be done in a variety of ways, as shown in [**Baiges2013**], in our case as a first approach it was decided to assemble and calculate the snapshots of each subdomain separately, this is $\boldsymbol{\phi}_{\mathrm{fl}}(\boldsymbol{u}_h, p_h)$ and $\boldsymbol{\phi}_{\mathrm{s}}(\boldsymbol{d}_h)$, but it is also possible to assemble just one base $\boldsymbol{\phi}_{\mathrm{fl,s}}(\boldsymbol{u}_h, p_h, \boldsymbol{d}_h)$, the effects of this is left for future study.

There have been many approaches to the solution of not only fluid problems by means of POD solution, for instance [**Sirovich1987**, **Carlberg2011**, **Baiges2014**], and very recently [**Reyes2018**], justifying our choice for the method.

4.1.2 VMS-ROM

Supposing that the ROM problem is variational we can assume it also requires the same stability conditions as the full order problem and benefits from any stabilization method. When we calculate the solution by means of the ROM problem (also known as on-line phase), following the same development as projection based stabilization methods, the residual of the solution of the governing equations is not projected unto a space orthogonal to the Finite Element (FE) one but rather to an orthogonal space to the ROM, where the solution is thought to belong. The whole formulation applied to ROM and its derivation is detailed in [**Reyes2018**]; The next few paragraphs describe the main idea of the method. Following the same analysis as in [**Codina2018**], we can define a variational version for the stabilized ROM problem shown in equation (7) as: find $\boldsymbol{U}_{\mathrm{rom}} :]0, t_{\mathrm{f}}[\longrightarrow \mathscr{Y}_{\mathrm{rom}}$ such that

$$
\begin{aligned}
&(\rho_{\mathrm{fl}} \partial_t \boldsymbol{u}_{\mathrm{rom}}^{n+1}, \boldsymbol{v}_{\mathrm{rom}}) + B(\boldsymbol{U}_{\mathrm{rom}}^{n+1}, \boldsymbol{V}_{\mathrm{rom}}) \\
&\qquad + \left(\Pi_{\mathrm{rom}}^{\perp} \left(\boldsymbol{r} \left(\boldsymbol{U}_{\mathrm{rom}}^{n+1} \right) \right), \boldsymbol{u}_{\mathrm{rom}}^{n+1} \cdot \nabla \boldsymbol{v}_{\mathrm{rom}} + \nu \Delta \boldsymbol{v}_{\mathrm{rom}} + \nabla q_{\mathrm{rom}} \right)_{\tau_{1,t}} \\
+ \left(\Pi_{\mathrm{rom}}^{\perp} \left(\nabla \cdot \boldsymbol{u}_{\mathrm{rom}}^{n+1} \right) \right), \nabla \cdot \boldsymbol{v}_{\mathrm{rom}} \Big)_{\tau_2} &= L(\boldsymbol{V}_{\mathrm{rom}}) + \frac{1}{\Delta t} \left(\breve{\boldsymbol{u}}^n, \boldsymbol{u}_{\mathrm{rom}}^n \cdot \nabla \boldsymbol{v}_{\mathrm{rom}} + \nu \Delta \boldsymbol{v}_{\mathrm{rom}} + \nabla q_{\mathrm{rom}} \right), \qquad (16)
\end{aligned}
$$

for $\boldsymbol{U}_{\mathrm{rom}} \equiv [\boldsymbol{u}_{\mathrm{rom}}, p_{\mathrm{rom}}] :]0, t_{\mathrm{f}}[\longrightarrow \mathscr{Y}_{\mathrm{rom}}$ and $\boldsymbol{V}_{\mathrm{rom}} \equiv [\boldsymbol{v}_{\mathrm{rom}}, q_{\mathrm{rom}}] \in \mathscr{Y}_{\mathrm{rom}}$, where initial conditions should hold and $\mathscr{Y}_{\mathrm{rom}}$ is the ROM space of variables, $\breve{\mathscr{Y}}$ is the space where the ROM sub-scales live, $\Pi_{\mathrm{rom}}^{\perp} := \mathbb{I} - \Pi_{\mathrm{rom}}$ in this case is the orthogonal projection on $\mathscr{Y}_{\mathrm{rom}}$, and $\mathbb{I}$ is now the identity in $\mathscr{Y}_{\mathrm{rom}}$. Notice that $\boldsymbol{\tau}_{\mathrm{K}}$ can be defined in the same manner as for the finite element space as it does not depend on the reduced model. In our case it has the same form as shown in equation (8).

Remark. *Note that the ROM stabilization is applied to the reduced problem in the same way as the FEM stabilization is applied to the full order model (FOM). This means that we do not apply ROM stabilization to the solid domain as our particular formulation does not require it.*

As a concluding remark on this section we would like to address our choice of not using modal analysis based methods, which is usually the norm for solid model reduction. It is clear that

fluid flow is impossible to represent via this kind of eigenvalue decomposition, specially the highly non-linear nature of the flows we are interested in. And even though it is possible to represent the non-linearities present in structural dynamics, as was mentioned in [**Thari2017**], a calculated basis by this approach needs to be recalculated every so often to guarantee that the solution will reproduce accurately non-linear behavior. Our approach focuses on the idea of "one for all" where by means of one robust formulation any kind of problem can be represented. In conclusion we apply the same form of decomposition (namely POD) for both fluid and structure.

4.2 The algorithm

Given our approach it is possible to run a wide variety of cases, of particular interest is running FSI-ROM-ROM, which in our context means a FSI case, applying a reduced order model in both fluid and solid at the same time. Obviously the same can be said for a FSI-FOM-FOM case, the counterpart of the previously described scenario, only both bases are constructed at the same time.

4.2.1 FOM-FOM case

The following algorithm, essentially the same algorithm shown in section 3.1.2 but with minor differences, depicts the off-line phase for a FOM-FOM case. We make use of all variables and parameters previously defined and add $\boldsymbol{\phi}_{\text{fl}}$ and $\boldsymbol{\phi}_{\text{s}}$; these are the fluid and solid basis respectively.

Read case parameters and initialize values for fluid and solid domains, number of snapshots to take and parameters for SVD solver
for $n = 1; n \leq n_{\text{last}}; n + 1$ **do**
  for $k = 1; k \leq k_{\max}; k + 1$ **do**
    ...
    for $i = 1; i \leq i_{\max}; i + 1$ **do**
      Solve fluid domain ...
    end for
    for $i = 1; i \leq i_{\max}; i + 1$ **do**
      Solve solid domain ...
    end for
    ...
    if $\epsilon_{\boldsymbol{u}}^{k+1}$ and ϵ_{p}^{k+1} and $\epsilon_{\boldsymbol{d}}^{k+1}$ on $\Gamma_{\text{I}} \leq \text{Tol}_{\text{coup}}$ **then**
      Store snapshot of $\boldsymbol{u}^{n+1}, p^{n+1}$ if required
      Store snapshot of $\boldsymbol{d}^{n+1}$ if required
      Coupling converged; Break Coupling loop
    end if
  end for
  ...
end for
Finalize case
Calculate base $\boldsymbol{\phi}_{\text{fl}}$, $\boldsymbol{\phi}_{\text{s}}$ by means of equation (14)
Output if necessary

Remark. *This process is most efficiently done taking full advantage of parallel solving, both for the FOM and ROM versions of the case. This means that the base can be calculated and written to disk in parallel as well.*

4.2.2 ROM-ROM case

The following algorithm depicts the ROM phase for the coupled problem, also known as on-line phase; we call this a ROM-ROM case. We make use of all parameters defined on section 4.2.1 and add $[\bar{\boldsymbol{u}}, \bar{p}, \bar{\boldsymbol{d}}]$ which are the snapshot mean values for fluid and solid sub-domains respectively.

Read general case parameters and values
Initialize Fluid problem: read previously calculated reduced basis $\boldsymbol{\phi}_{\text{fl}}$, and select the desired amount of basis vectors through any criteria (energy for example).
Initialize Solid problem: read previously calculated reduced basis $\boldsymbol{\phi}_{\text{s}}$, and select the desired amount of basis vectors through any criteria (energy for example).
for $n = 1; n \leq n_{\text{last}}; n+1$ **do**
  for $k = 1; k \leq k_{\max}; k+1$ **do**
    Calculate relaxation parameter ω_{k+1} for Γ_{I} from $\boldsymbol{r}_{\Gamma_{\text{I}},k+1}$
    Calculate mesh interface movement $\boldsymbol{d}_{\Gamma_{\text{I}}}^{k+1} = \boldsymbol{d}_{\Gamma_{\text{I}}}^{k} + \omega_{k+1}\boldsymbol{r}_{\Gamma_{\text{I}},k+1}$
    Calculate mesh movement $\boldsymbol{d}_{\text{mesh}}^{k+1}$ and velocity $\boldsymbol{u}_{\text{mesh}}^{k+1}$ from $\boldsymbol{d}_{\Gamma_{\text{I}}}^{k+1}$
    for $i = 1; i \leq i_{\max}; i+1$ **do**
      Solve Fluid domain for $[\boldsymbol{u}, p]_{\text{rom}}^{i+1}$ from $\boldsymbol{u}_{\text{mesh}}^{k+1}$
      Project to $\mathscr{F}_{D,t}$ space: $[\boldsymbol{u}, p] \approx [\bar{\boldsymbol{u}}, \bar{p}] + \sum_{k=1}^{m} [\boldsymbol{u}, p]_{\text{rom}} \boldsymbol{\phi}_{\text{fl}}^{k}$
      Calculate tractions $\boldsymbol{t}_{\text{fl}}$ on Γ_{I}
      Calculate error $\epsilon_{\boldsymbol{u}}^{i+1} = \frac{|\boldsymbol{u}^{i+1} - \boldsymbol{u}^{i}|}{|\boldsymbol{u}^{i+1}|}$; $\epsilon_{p}^{i+1} = \frac{|p^{i+1} - p^{i}|}{|p^{i+1}|}$;
      if $\epsilon_{\boldsymbol{u}}^{i+1}$ and $\epsilon_{p}^{i+1} \leq \text{Tol}_{\text{fl}}$ **then**
        Non linearity converged; Break non-linearity loop
      end if
    end for
    for $i = 1; i \leq i_{\max}; i+1$ **do**
      Solve Solid domain for $\boldsymbol{d}_{\text{rom}}^{i+1}$ from $\boldsymbol{t}_{\text{fl}}$
      Project to $\mathscr{F}_{D,t}$ space: $\boldsymbol{d} \approx \bar{\boldsymbol{d}} + \sum_{k=1}^{m} \boldsymbol{d}_{\text{rom}} \boldsymbol{\phi}_{\text{s}}^{k}$
      Calculate error $\epsilon_{\boldsymbol{d}}^{i+1} = \frac{|\boldsymbol{d}^{i+1} - \boldsymbol{d}^{i}|}{|\boldsymbol{d}^{i+1}|}$
      if $\epsilon_{\boldsymbol{d}}^{i+1} \geq \text{Tol}_{\text{s}}$ **then**
        Non linearity converged; Break non-linearity loop
      end if
    end for
    Calculate coupling error $\epsilon_{\boldsymbol{u}}^{k+1} = \frac{|\boldsymbol{u}^{k+1} - \boldsymbol{u}^{k}|}{|\boldsymbol{u}^{k+1}|}$; $\epsilon_{p}^{k+1} = \frac{|p^{k+1} - p^{k}|}{|p^{k+1}|}$; $\epsilon_{\boldsymbol{d}}^{k+1} = \frac{|\boldsymbol{d}^{k+1} - \boldsymbol{d}^{k}|}{|\boldsymbol{d}^{k+1}|}$
    if $\epsilon_{\boldsymbol{u}}^{k+1}$ and ϵ_{p}^{k+1} and $\epsilon_{\boldsymbol{d}}^{k+1}$ on $\Gamma_{\text{I}} \leq \text{Tol}_{\text{coup}}$ **then**
      Coupling converged; Break Coupling loop
    end if
  end for
  Calculate temporal error $\epsilon_{\boldsymbol{u}}^{n+1} = \frac{|\boldsymbol{u}^{n+1} - \boldsymbol{u}^{n}|}{|\boldsymbol{u}^{n+1}|}$; $\epsilon_{p}^{n+1} = \frac{|p^{n+1} - p^{n}|}{|p^{n+1}|}$; $\epsilon_{\boldsymbol{d}}^{n+1} = \frac{|\boldsymbol{d}^{n+1} - \boldsymbol{d}^{n}|}{|\boldsymbol{d}^{n+1}|}$
  if $\epsilon_{\boldsymbol{u}}^{n+1}$ and ϵ_{p}^{n+1} and $\epsilon_{\boldsymbol{d}}^{n+1} \leq \text{Tol}_{\text{time}}$ **then**
    Stationary state achieved; Break temporal loop
  end if
end for
Finalize case
Output if necessary

Remark. *Again note that this process is most efficient taking advantage of parallel computing.*

5 Numerical Results

In this section FSI-ROM-ROM case results are shown. Two main problems were analyzed which exemplify most cases of interest, this being a semi-stationary case and a fully developed FSI case. For the fluid domain generally plots of integral quantities are preferred (lift and/or drag), pressure in the case of the semi-stationary case. For the solid domain displacement and acceleration plots are ussually shown. A Fourier transform of the results will be presented whenever deemed necessary. Regarding the ROM problem, results will be presented comparing the ROM result with the FOM result for the same case, using the basis that produced the most accurate results. Basis energy percentage is used for comparison between ROM results. Notice that in this work, each case consists of two reduced problems, each with its particular basis taken from different amount of snapshots. It was seen that the ROM cases require greater stabilization for the incompressibility term to guarantee accurate results, see equation (8c). For all FOM cases this constant has a value of $c_3 = 1.0$. On section 5.2 we explore the effect of a slight variation of this constant.

5.1 Semi-stationary bending of FSI plate

This 2D semi-stationary problem, taken from [**Baiges2011**], consists of a clamped plate perpendicular to the fluid flow. Once the flow starts from the left wall it will bend the plate. For the particular conditions of the test, a force balance between the tractions imposed by the fluid and the stress on the plate will be achieved where the plate will remain bent without oscillation. The test conditions are shown in table 1. In this example, all ROM cases are solved using constant $c_3 = 2.0$ in the ROM equation corresponding to equation (8c).

Table 1: Physical parameters

	Fluid		Solid
ρ_{fl}	2.0	ρ_{s}	10.0
ν_{fl}	0.2	μ_{s}	5,000
		λ_{s}	2,000
model	Newtonian		Neo-Hookean

Figure 2 shows the geometry and mesh for the test, where $H = 20$, $L = 80$, $h = 1$, $l = 10$.

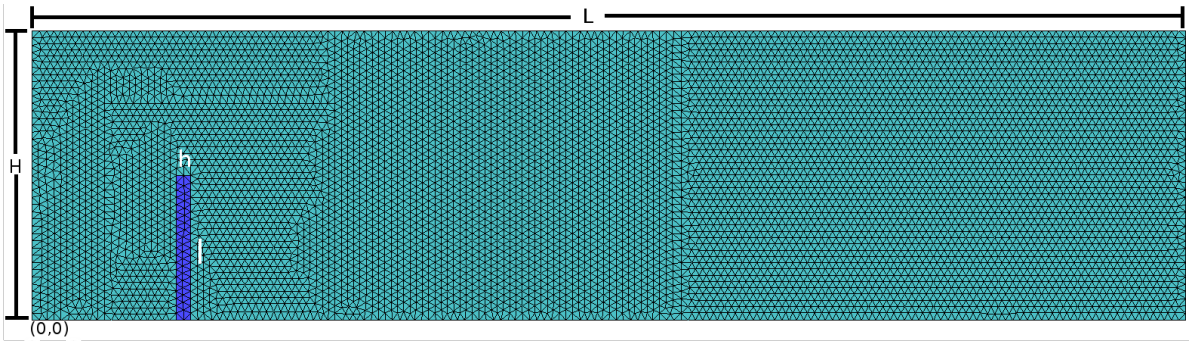

Figure 2: Geometry and mesh used for semi-stationary FSI-ROM case

Table 2 shows important mesh parameters and boundary conditions.

Table 2: Mesh parameters

	Fluid	Solid
Element type	Quad-Triangular	Quad-Triangular
nodes/element	6	6
total elements	14,308	78
total nodes	29,057	201

Table 3: Boundary conditions

	Fluid	Solid
X = 0	$u_x = 1.0$, $u_y = 0.0$	$d_x = d_y = 0.0$
Y = 0, Y = H	Free slip	
X = L	Free	
other boundaries		Free

Out of experimentation it was found that ROM results that accurately represent the full order model is when 99.999999% of the energy of the fluid base is taken, amounting to 150 basis vectors, and 99.999999% of the energy of the solid base is taken, amounting to 36 basis vectors.

Notice that from table 2 it can be calculated that for the fluid problem the amount of degrees of freedom (DOF) is 87,171 while for the solid is 402. For the reduced problem we have 150 DOF for the fluid and 36 for the solid. This means that overall in terms of DOF we are achieving a reduction of 99.83% for the fluid and 91.05% for the solid, for a total reduction of 99.79%.

Figures 3 and 4 shows contour plots for velocity and Figures 5 and 6 shows contour plots for pressure for the final time-step of analysis, $t_f = 10.0$s.

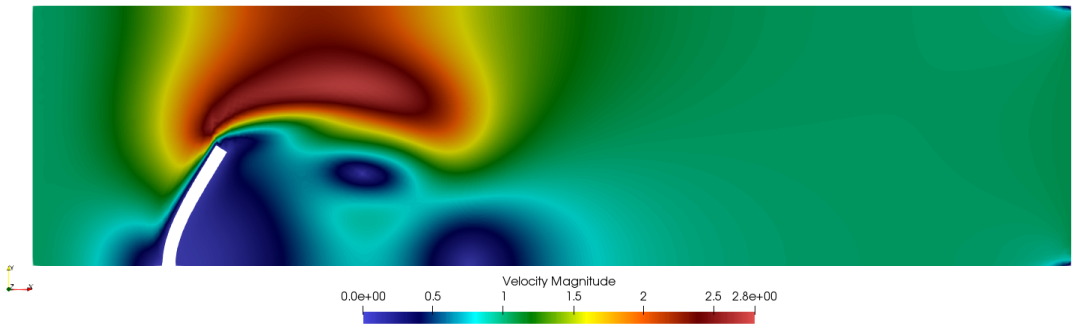

Figure 3: FOM - Velocity

It is easy to note that both solutions, FOM and ROM, are very similar for both fluid and solid. In this regard it is easier to analyze the data from the following plots. Out of the many results collected we consider valuable to see the dependency of the basis on the amount of time that was sampled. Results are shown for three particular cases, $\boldsymbol{\phi}_{\text{ROM\_A}}$ which was calculated taking a snapshot every time step during a time interval $t(0, 10s)$, $\boldsymbol{\phi}_{\text{ROM\_B}}$ which was calculated taking a snapshot every time step during a time interval $t(0, 20s)$ and $\boldsymbol{\phi}_{\text{ROM\_C}}$ which was calculated taking a snapshot every time step during a time interval $t(0, 40s)$. Results are thus shown for problem ROM_A which was solved by means of basis $\boldsymbol{\phi}_{\text{ROM\_A}}$, problem ROM_B which was solved by means of basis $\boldsymbol{\phi}_{\text{ROM\_B}}$ and problem ROM_C which was solved by means of basis $\boldsymbol{\phi}_{\text{ROM\_C}}$.

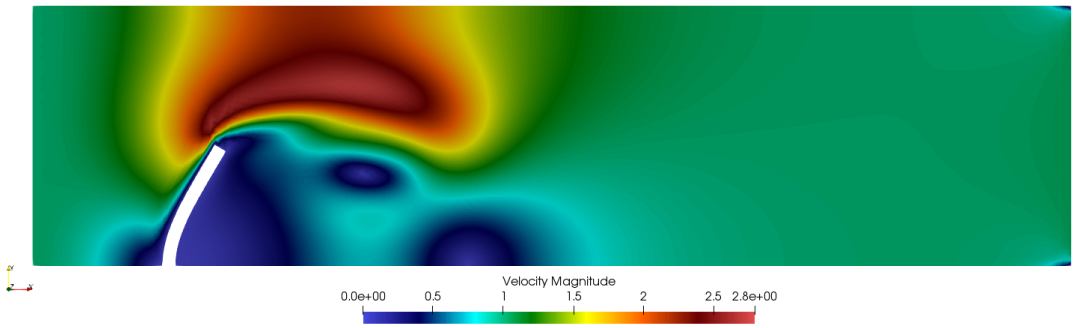

Figure 4: ROM - Velocity

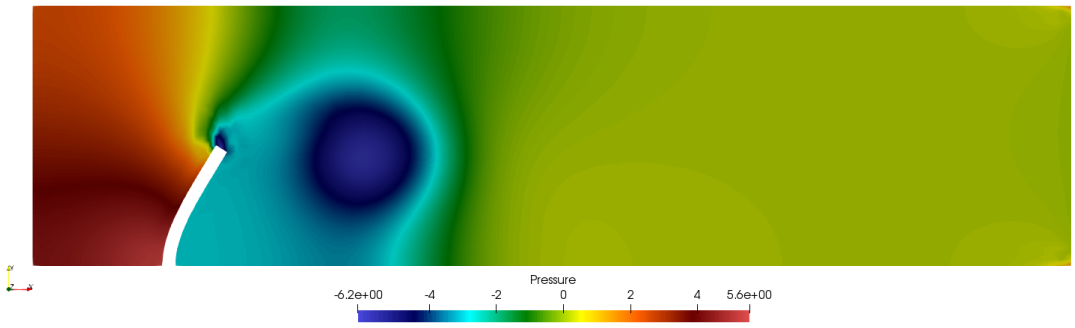

Figure 5: FOM - Pressure

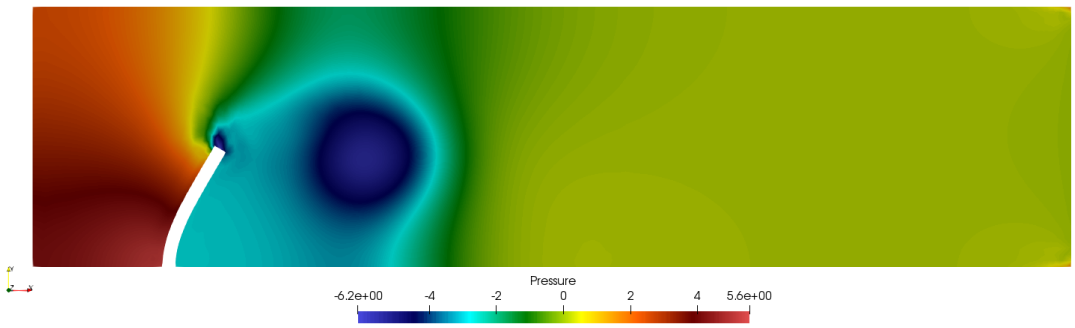

Figure 6: ROM - Pressure

Figures 8 and 9 show the velocities and pressure on a point above the flag. Notice the importance of sampling the long stationary that develops after second 12. Even though cases ROM_B and ROM_C produce similar results, Figure 9b highlights ROM_C as a more stable and smoother solution.

Figure 10 shows the displacement of the tip of the flag, once again it is important to notice that lack of sampling of the stationary part of the solution makes the ROM inaccurate only in this region.

Figures 11 and 12 shows the acceleration and its Fourier's transform for the tip of the flag. The analysis of the acceleration of the solid has been found to be critical specially for FSI cases. It is this quantity that is really telling of the stability of the solid domain; ROM_C points once again to a more accurate solution.

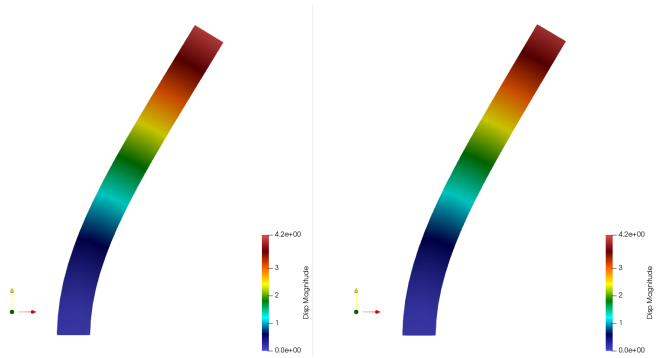

Figure 7: Displacement magnitude for the solid bar, Left FOM, right ROM

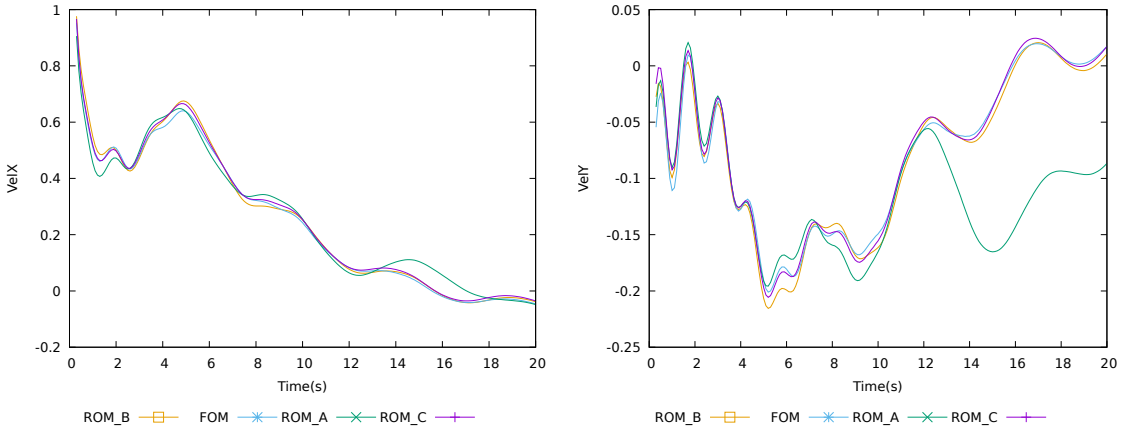

(a) Velocity in x axis

(b) Velocity in y axis

Figure 8: x and y velocities above the plate

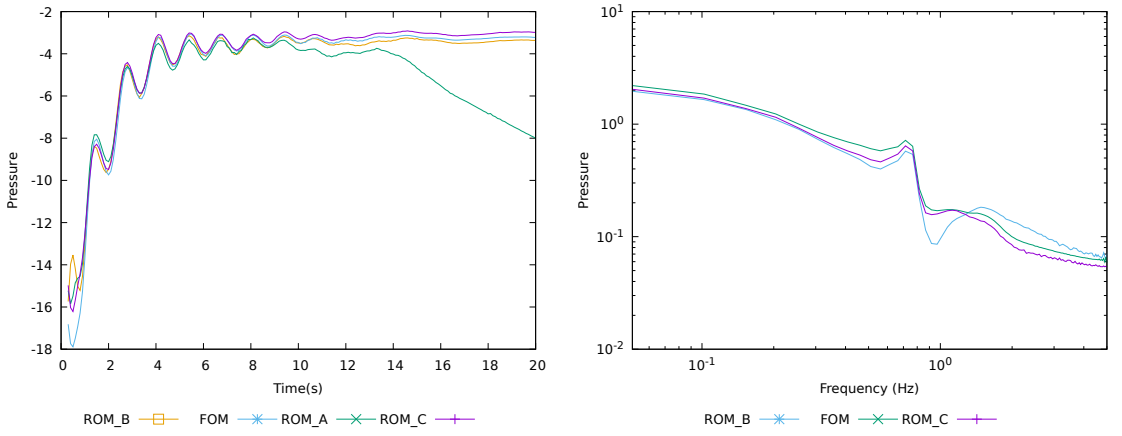

(a) Pressure

(b) Pressure FFT

Figure 9: Pressure and its FFT around the plate

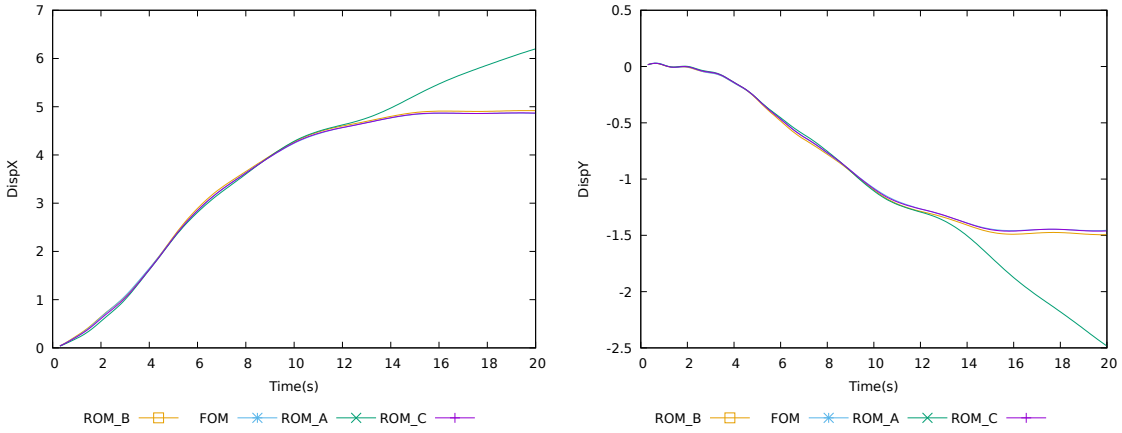

(a) Displacement in x axis

(b) Displacement in y axis

Figure 10: Displacement of the tip of the plate

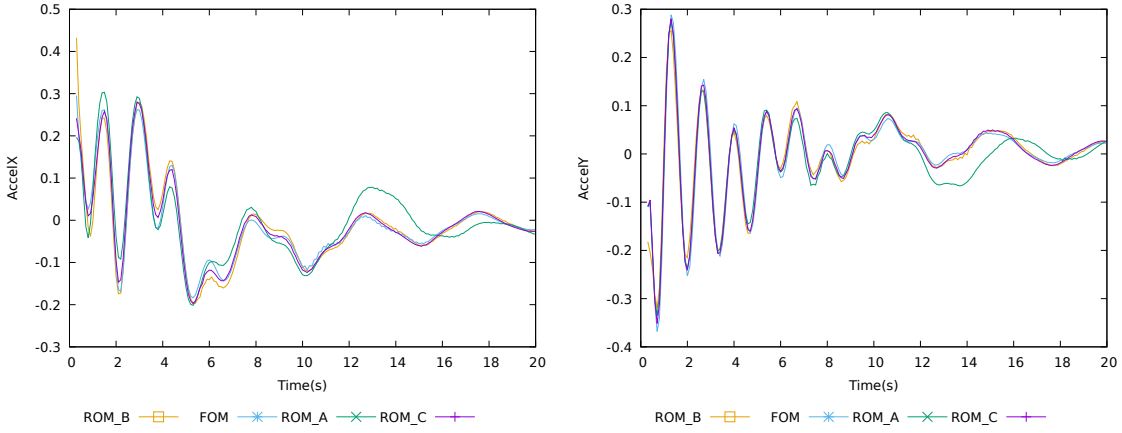

(a) Acceleration in x axis

(b) Acceleration in y axis

Figure 11: Acceleration of the tip of the plate

5.2 Flow around a cylinder with supported flag

The following example is reproduces the benchmark shown in [**Hron2006**] where a fluid flows around a cylinder with a supported flag. The fluid flows from the left wall and initially the tractions of the fluid onto the solid initiate the flag motion. After a while this motion is significant enough to move the fluid around it, starting a feedback loop between fluid and solid. The test conditions are shown in table 4.

Figures 13 and 14 show the mesh and geometry used in this example. Note that the solid and fluid meshes are non-conforming making use of interpolation between sub-domains necessary as discussed in section 3.1.1. The length of the fluid domain is $L = 2.5$, its height $H = 0.41$, and the radius of the circle $R = 0.05$. $l = 0.35$ is the length of the bar, and $h = 0.02$ its thickness.

Figure 15 shows a zoom for the cylinder and bar.

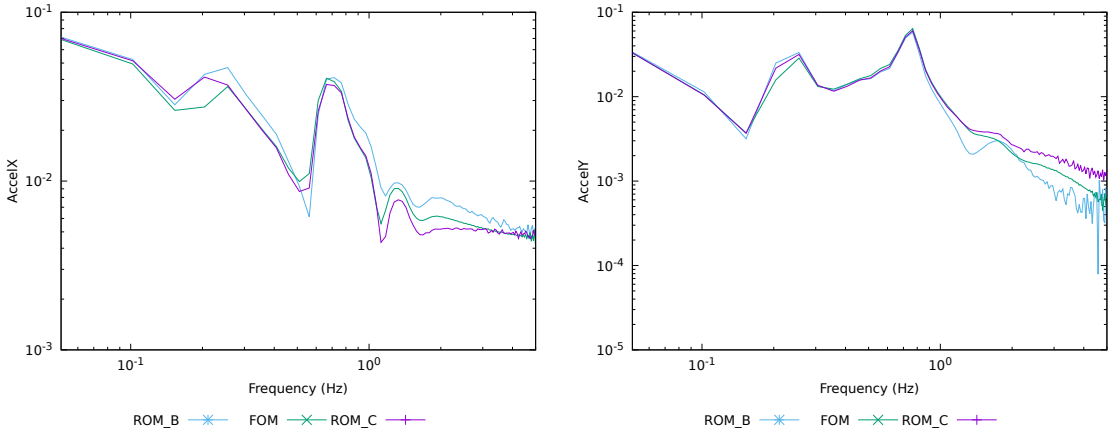

(a) Acceleration FFT in x axis

(b) Acceleration FFT in y axis

Figure 12: FFT of the Acceleration of the tip of the plate

Table 4: Physical parameters

	Fluid		Solid
ρ_{fl}	1,000.0	ρ_{s}	10,000.0
ν_{fl}	0.001	μ_{s}	1.929e6
		λ_{s}	7.714e6
model	Newtonian		St.Venant-Kirchoff

Figure 13: Geometry

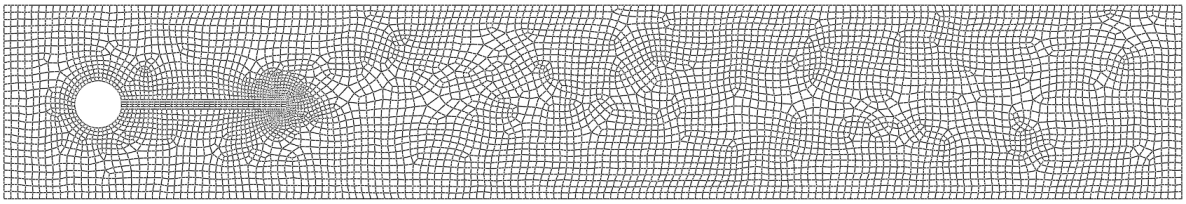

Figure 14: Non-conforming mesh

Tables 5 and 6 show important mesh parameters and boundary conditions respectively.

Out of experimentation it was found that ROM results that accurately represent the full order model is when 99.999999% of the energy of the fluid base is taken, amounting to 163 basis vectors, and 99.999999% of the energy of the solid base is taken, amounting to 48 basis vectors. Results for a base using 99.9999% of the energy are also shown using 158 basis vector for the fluid and 16 for

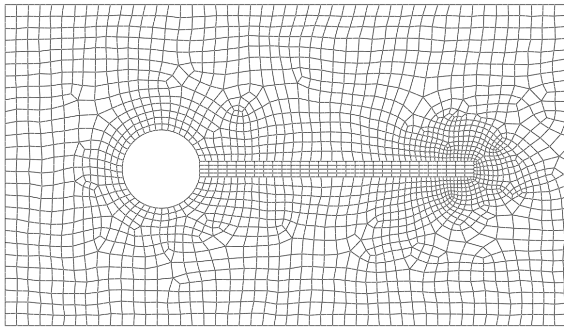

Figure 15: Non-conforming mesh - zoom

Table 5: Mesh parameters

	Fluid	Solid
Element type	Quadratic-Quads	Quadratic-Quads
nodes/element	9	9
total elements	5,531	500
total nodes	22,642	2,211

Table 6: Boundary conditions

	Fluid	Solid
$x = 0$	$u_x = 35.693\, y(0.41 - y)$, $u_y = 0.0$	
$y = 0$, $y = \mathrm{H}$	Free slip	
$x = \mathrm{L}$	Free	
cylinder	No slip	
bar	No slip	Free
left side of bar		$d_x = d_y = 0.0$

the solid.

Notice that from table 5 it can be calculated that for the fluid problem the amount of degrees of freedom (DOF) is 67,926 while for the solid is 4422. For the reduced problem we have 163 DOF for the fluid and 48 for the solid. This means that overall in terms of DOF we are achieving a reduction of 99.76% for the fluid and 98.91% for the solid, for a total reduction of 99.71%.

The following collection of figures show contours for velocity, sub-grid scales and pressure, for both the reduced order problem and the full order problem at the last time of the simulation $t = 1.2$. After this, graphs of significant quantities will be compared for both the reduced and full order problem.

Figures 16 and 17 show velocity contours, Figures 18 and 19 show the pressure contours for both fluid problems, and Figure 20 shows in this case the strain contours for the solid domain for both problems; solutions are very similar.

Out of the many results obtained it is considered valuable to see the dependency of the ROM result on the energy percentage used. Results are shown for three particular cases, ROM_A($\eta = 99.9999\%$),ROM_B($\eta = 99.9999\%$), ROM_C($\eta = 99.999999\%$). A snapshot was taken every time-step. The basis for all three cases was obtained sampling every time-step of the FOM solution.

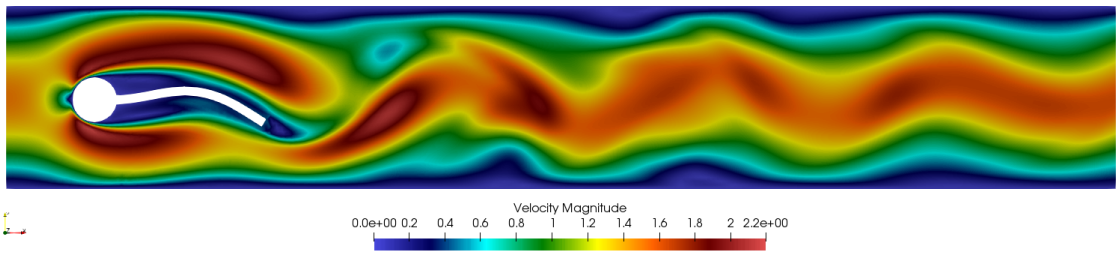

Figure 16: FOM - Velocity magnitude

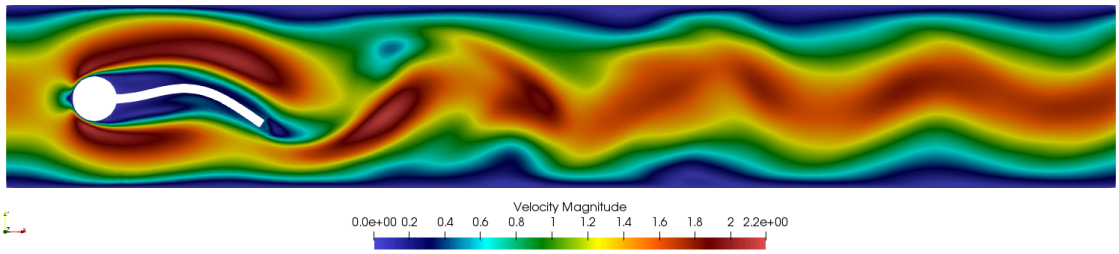

Figure 17: ROM - Velocity magnitude

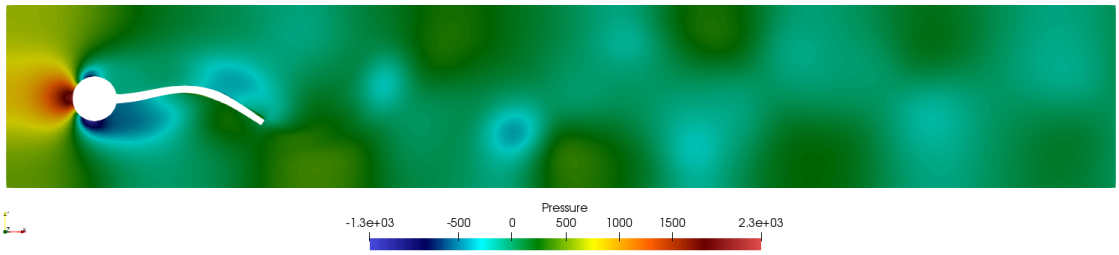

Figure 18: FOM - Pressure

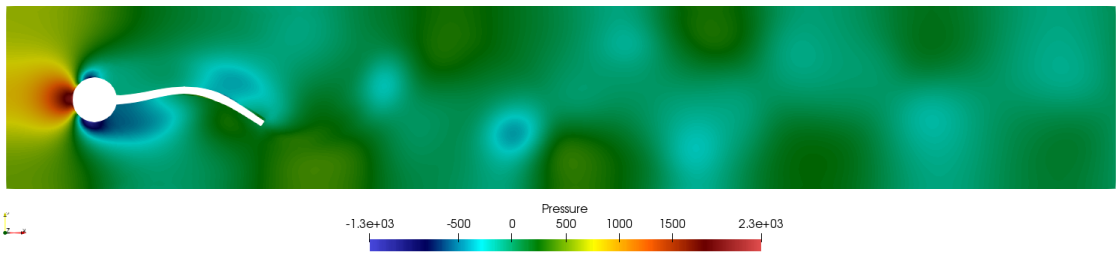

Figure 19: ROM - Pressure

While cases ROM_A($\eta = 99.9999\%$) and ROM_B($\eta = 99.9999\%$) share the same basis and same energy percentage the crucial difference between cases is the stabilization constant for the incompressibility term for the Navier-Stokes equation. In this example we explore the effect of a slight variation in constant c_3. For case ROM_A $c_3 = 1.5$ while for ROM_B $c_3 = 2.0$.

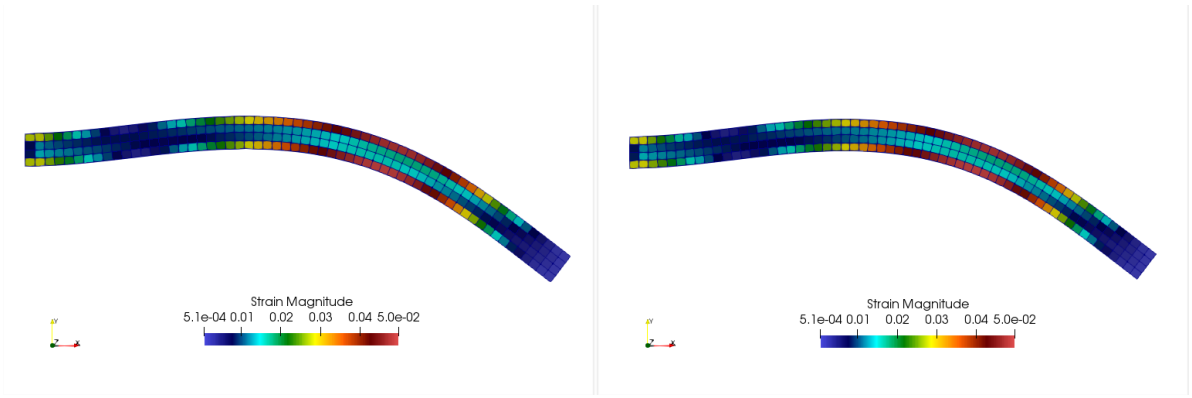

Figure 20: Strain magnitude for the solid bar, Left FOM, right ROM

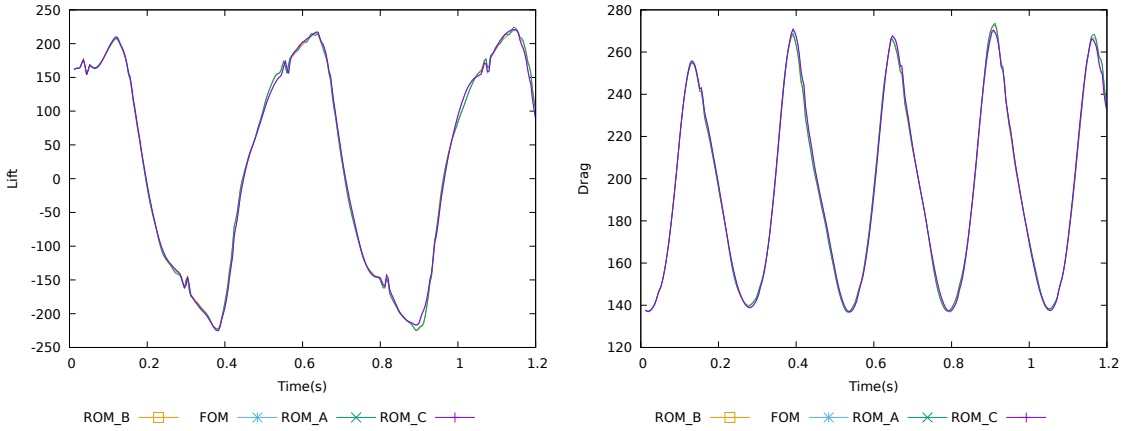

(a) Lift (b) Drag

Figure 21: Lift and drag around the cylinder and flag

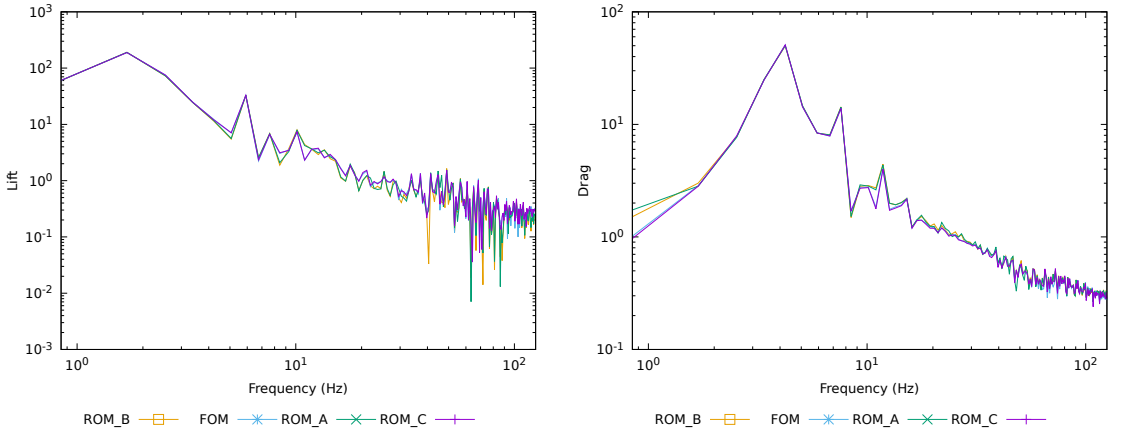

(a) Lift FFT (b) Drag FFT

Figure 22: FFT of the lift and drag around the cylinder and flag

Figures 21 and 22 show the drag and lift around the geometry of the flag caused by the fluid. Unlike the example shown in section 5.1 this test case is much more complex and requires much more computation time as well as a richer base to reproduce meaningful results.

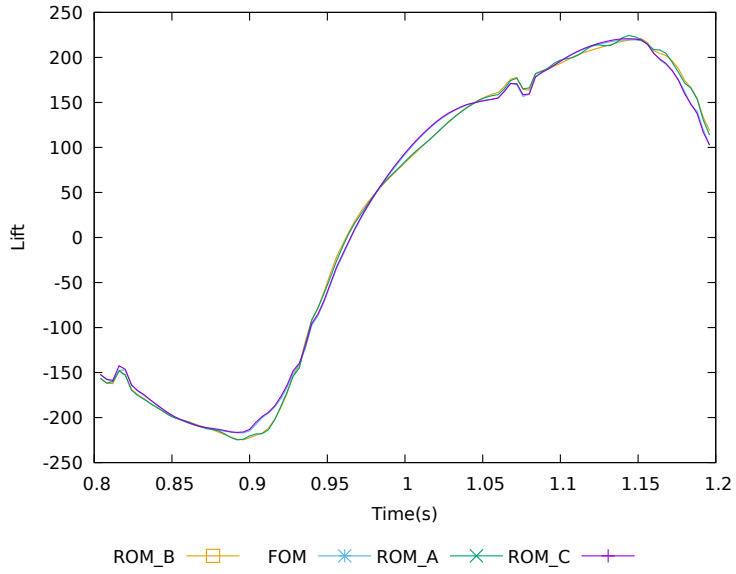

Figure 23: Zoom for lift

Figure 23 shows a zoom for the lift around the geometry of the flag.

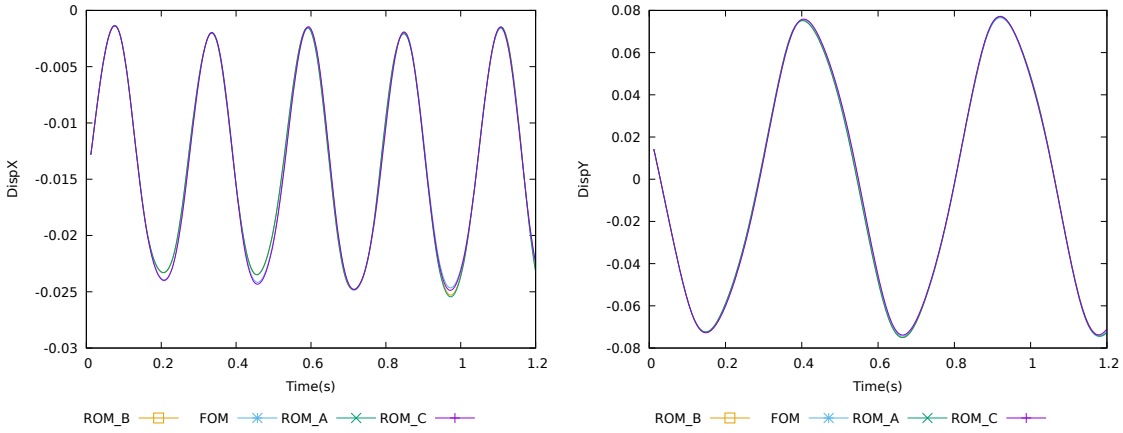

(a) Displacement in x axis

(b) Displacement in y axis

Figure 24: Displacement of the tip of the flag

Figures 24 and 25 show the displacement and its Fourier's transform for the tip of the flag, all results reproduce accurately the FOM.

Figures 26 and 27 show the acceleration and its Fourier's transform for the tip of the flag. In this case the analysis of the acceleration of the flag is not only interesting but crucial, it can be seen that taking a higher stabilization constant for the incompressibility term changes the accuracy by which a ROM case reproduces the FOM. This fact is crucial as this leads to higher speedup for the

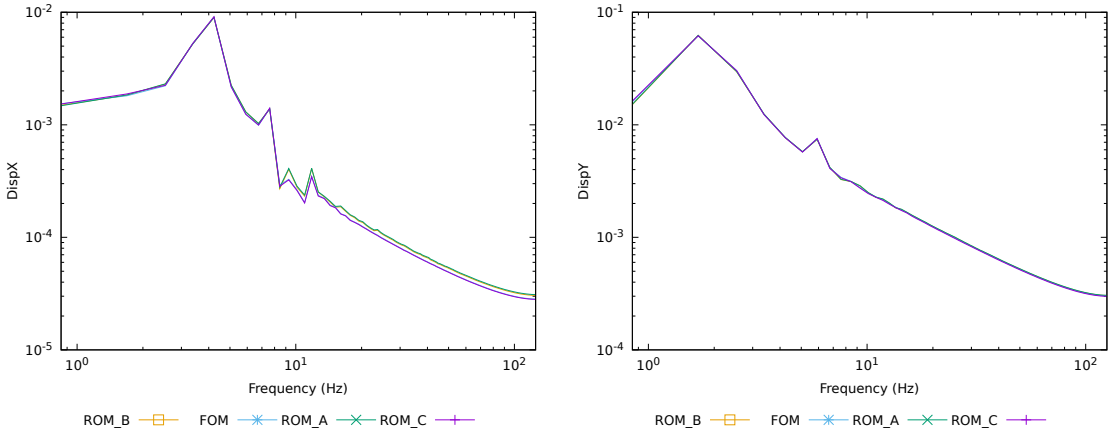

(a) Displacement FFT in x axis

(b) Displacement FFT in y axis

Figure 25: FFT of the displacement of the tip of the flag

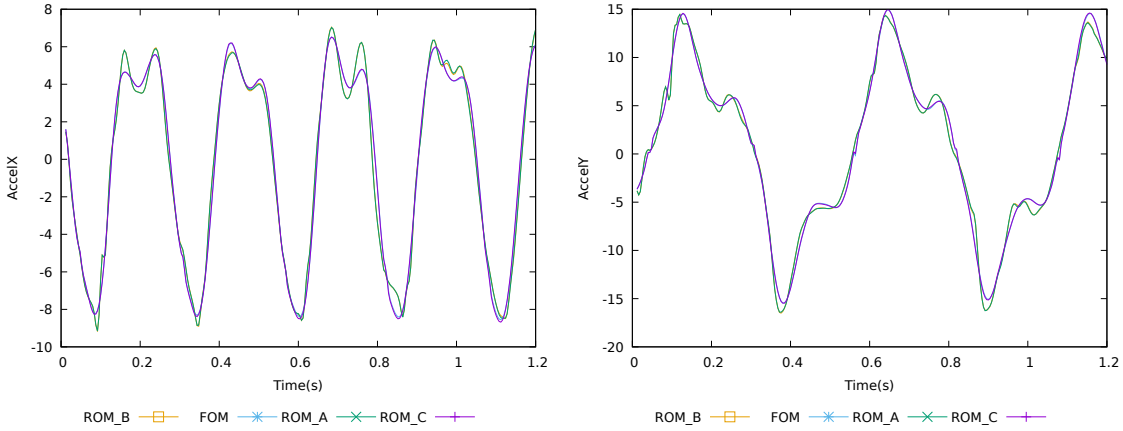

(a) Acceleration in x axis

(b) Acceleration in y axis

Figure 26: Acceleration of the tip

same accuracy.

Table 7 shows the total times and speedup for all cases shown; notice that times shown are in minutes.

Table 7: Time and speedup for fluid and solid domains

		FOM	ROM_A	ROM_B	ROM_C
Fluid	Time(min)	88.53	16.21	19.33	18.94
	Speedup		81.69%	78.16%	78.6%
Solid	Time(min)	0.79	0.54	0.63	0.684
	Speedup		31.65%	20.25%	13.42%
Total	Time(min)	89.32	16.75	19.96	19.624
	Speedup		81.24%	77.65%	78.3%

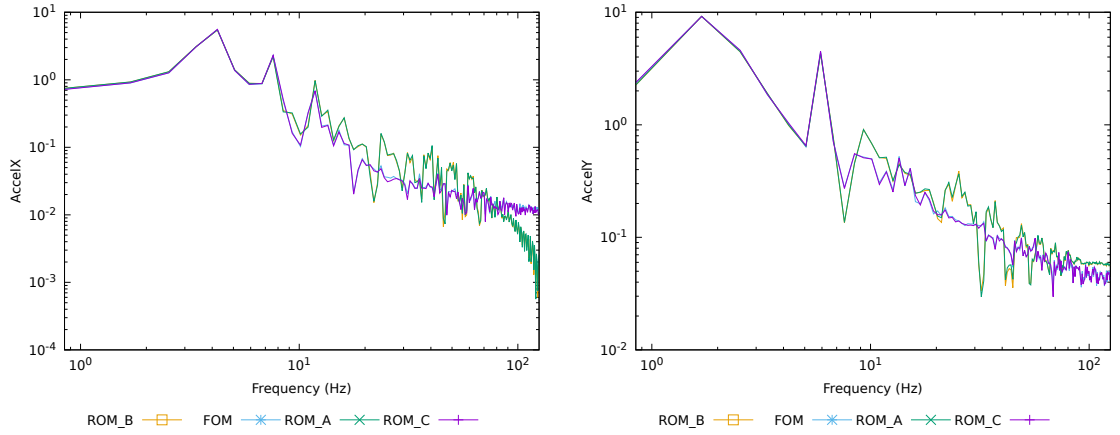

(a) Acceleration FFT in x axis

(b) Acceleration FFT in y axis

Figure 27: FFT of the acceleration of the tip of the flag

As it can be observed speedup has been achieved for a more complex case involving fully transitory interaction.

6 General conclusions

In comparison to the work done by [**Reyes2018**], where the cases shown could be solved with a basis energy in the range of 80% to 95%, FSI problems look to be much more sensitive to the amount of energy in the basis necessary to achieve solution. It was found that even for the simplest of cases the problem would not produce any valuable solution with an energy percentage under 99.0%, still producing a significant speed up for both fluid and solid. A priori it is possible that this hints to the importance of the high frequencies of the base spectrum in the solution of a FSI problem. This remains to be studied further and it is an interesting topic for future work.

Partitioned FSI problems have a series of restrictions, such as a maximum time step and added diffusivity, that must be met so as to minimize the effect of the instabilities like the added mass effect. This in turn is also a restriction on the reduced model, making FSI-ROM cases very dependent on how often a snapshot is taken to be able to capture enough of the physics of the problem while keeping instabilities out of the sampling. A richer base consists of more basis vectors that contain higher frequencies, and in turn, produce a better approximation to the full order model problem. Again, correlating with the above, this hints to the dependency on the high frequency low energy modes at the end of the spectrum of the basis.

ROM problems with a higher stabilization constant for the incompressibility produced more accurate results that their counterparts with a lower ones. Taking $c_3 = 1.0$ (the value used for the FOM) produces spurious results with loss of amplitude through time and off phase (in comparison to the FOM).

As expected speedup has been achieved for all cases presented with accurate results.

Acknowledgements

Alexis Tello wants to acknowledge the doctoral scholarship received from the Colombian government-Colciencias. Ramon Codina acknowledges the support received from the ICREA Acadèmia Research Program of the Catalan Government. Joan Baiges acknowledges the support of the Spanish Government through the Ramón y Cajal grant RYC-2015-17367. This work is partially funded through the ELASTIC-FLOW project, Ref. DPI2015-67857-R of the Spanish Government.